

Charge carrier transport properties in layer structured hexagonal boron nitride

T. C. Doan, J. Li, J. Y. Lin, and H. X. Jiang^a

*Department of Electrical and Computer Engineering, Texas Tech University,
Lubbock, Texas 79409, USA*

(Received 2 September 2014; accepted 3 October 2014; published online 14 October 2014)

Due to its large in-plane thermal conductivity, high temperature and chemical stability, large energy band gap (~ 6.4 eV), hexagonal boron nitride (*h*BN) has emerged as an important material for applications in deep ultraviolet photonic devices. Among the members of the III-nitride material system, *h*BN is the least studied and understood. The study of the electrical transport properties of *h*BN is of utmost importance with a view to realizing practical device applications. Wafer-scale *h*BN epilayers have been successfully synthesized by metal organic chemical deposition and their electrical transport properties have been probed by variable temperature Hall effect measurements. The results demonstrate that undoped *h*BN is a semiconductor exhibiting weak p-type at high temperatures (> 700 °K). The measured acceptor energy level is about 0.68 eV above the valence band. In contrast to the electrical transport properties of traditional III-nitride wide bandgap semiconductors, the temperature dependence of the hole mobility in *h*BN can be described by the form of $\mu \propto (T/T_0)^{-\alpha}$ with $\alpha = 3.02$, satisfying the two-dimensional (2D) carrier transport limit dominated by the polar optical phonon scattering. This behavior is a direct consequence of the fact that *h*BN is a layer structured material. The optical phonon energy deduced from the temperature dependence of the hole mobility is $\hbar\omega = 192$ meV (or 1546 cm^{-1}), which is consistent with values previously obtained using other techniques. The present results extend our understanding of the charge carrier transport properties beyond the traditional III-nitride semiconductors. © 2014 Author(s). All article content, except where otherwise noted, is licensed under a Creative Commons Attribution 3.0 Unported License. [<http://dx.doi.org/10.1063/1.4898630>]

I. INTRODUCTION

Among the members of the III-nitride material system, hexagonal boron-nitride (*h*BN) is the least studied and understood. Its extraordinary physical properties, such as ultra-high chemical stability, thermal conductivity, electrical resistivity, and band gap ($E_g \sim 6.4$ eV) make *h*BN the material of choice for emerging applications such as deep ultraviolet (DUV) optoelectronic devices.¹⁻⁷ Moreover, due to its complementarity and close lattice match to graphene, *h*BN has recently attracted considerable attention for the exploration of van der Waals heterostructures consisting of *h*BN/graphene with new physics and applications.^{8,9} The large thermal neutron capture cross-section (3840 barns) of ^{10}B ^{10,11} also makes *h*BN potentially a very promising material for the realization of solid-state neutron detectors.^{12,13}

The knowledge and experimental data on the electrical transport properties of *h*BN are scarce due partly to its very large bandgap and highly electrical insulating nature. An improved understanding of the electrical properties of *h*BN is necessary to take the advantages of its excellent physical properties for significant device applications. Our present studies focus on the electrical transport properties of unintentionally doped *h*BN epitaxial layers (or epilayers) grown by metal organic chemical vapor deposition (MOCVD). In contrast to traditional III-nitride semiconductors,

^ahx.jiang@ttu.edu



it was observed that the mobility versus temperature behavior in *h*BN is governed by 2D effects due to its unique layered structure. Experimental results suggest that the scattering mechanism is dominated by carrier polar optical phonon interaction at high temperatures. The optical phonon energy deduced from the temperature dependence of the hole mobility is consistent with values previously obtained using other methods.

II. EXPERIMENT AND BASIC CHARACTERISTICS OF *h*BN EPILAYERS

The *h*BN epilayer structure used in this study is schematically illustrated in Fig. 1(a). The *h*BN epilayers were grown on *c*-plane sapphire substrates by MOCVD using hydrogen as a carrier gas. MOCVD is an established technique for producing high quality crystalline materials due to its ability to precisely control the growth processes and has been widely adopted by the commercial sector for producing III-nitride wide bandgap semiconductors in large wafer scales.¹⁴ The precursors for boron and nitrogen are tri-ethyl boron (TEB) and ammonia (NH₃), respectively. For the growth of *h*BN epilayers, the typical V/III ratio employed was around 3000 and a pulsed growth scheme (alternating flows of TEB and NH₃) was undertaken to minimize the pre-reaction between TEB and ammonia, which is necessary for obtaining epilayers in hexagonal phase.¹⁵ Adopted from the hetero-epitaxial growth of III-nitride device structures, a low temperature BN buffer layer of about 10 nm in thickness was deposited on the sapphire substrate at about 800 °C prior to the growth of *h*BN epilayer. The growth temperature used to produce *h*BN epilayers reported in this work was around 1300 °C. The Hall effect measurements were conducted to measure the charge carrier type, concentration, mobility, and conductivity of *h*BN epilayers.

Figure 1(b) is an atomic force microscopy (AFM) image over a $2 \times 2 \mu\text{m}^2$ area scan, indicating that it is possible to obtain *h*BN epilayers with a good surface morphology (RMS value around 1 nm). The θ - 2θ scan of X-ray diffraction (XRD) of *h*BN epilayers is shown in Fig. 1(c). All three peaks corresponding to the *h*BN (002), (004), and (006) reflections were clearly identified at 26.70°,

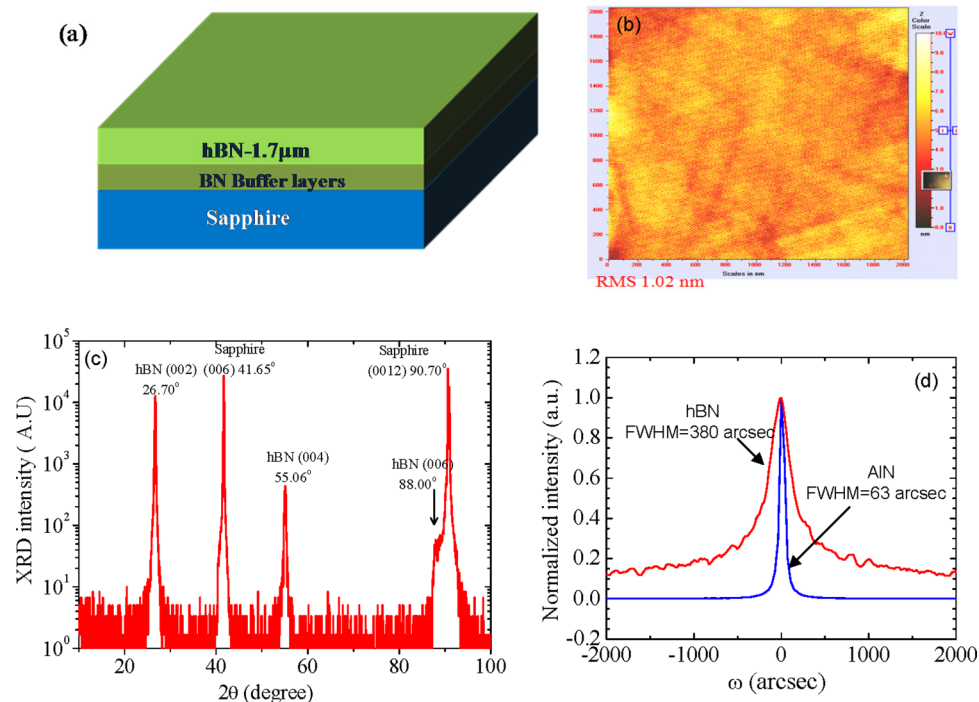


FIG. 1. (a) Schematic layer structure of the *h*BN epilayer used in this study; (b) AFM image of *h*BN epilayer over a $2 \times 2 \mu\text{m}^2$ area scan; (c) XRD θ - 2θ scan of the *h*BN epilayer used in this study; and (d) Comparison of XRD rocking curves of the (0002) diffraction peaks of *h*BN and AlN epilayers.

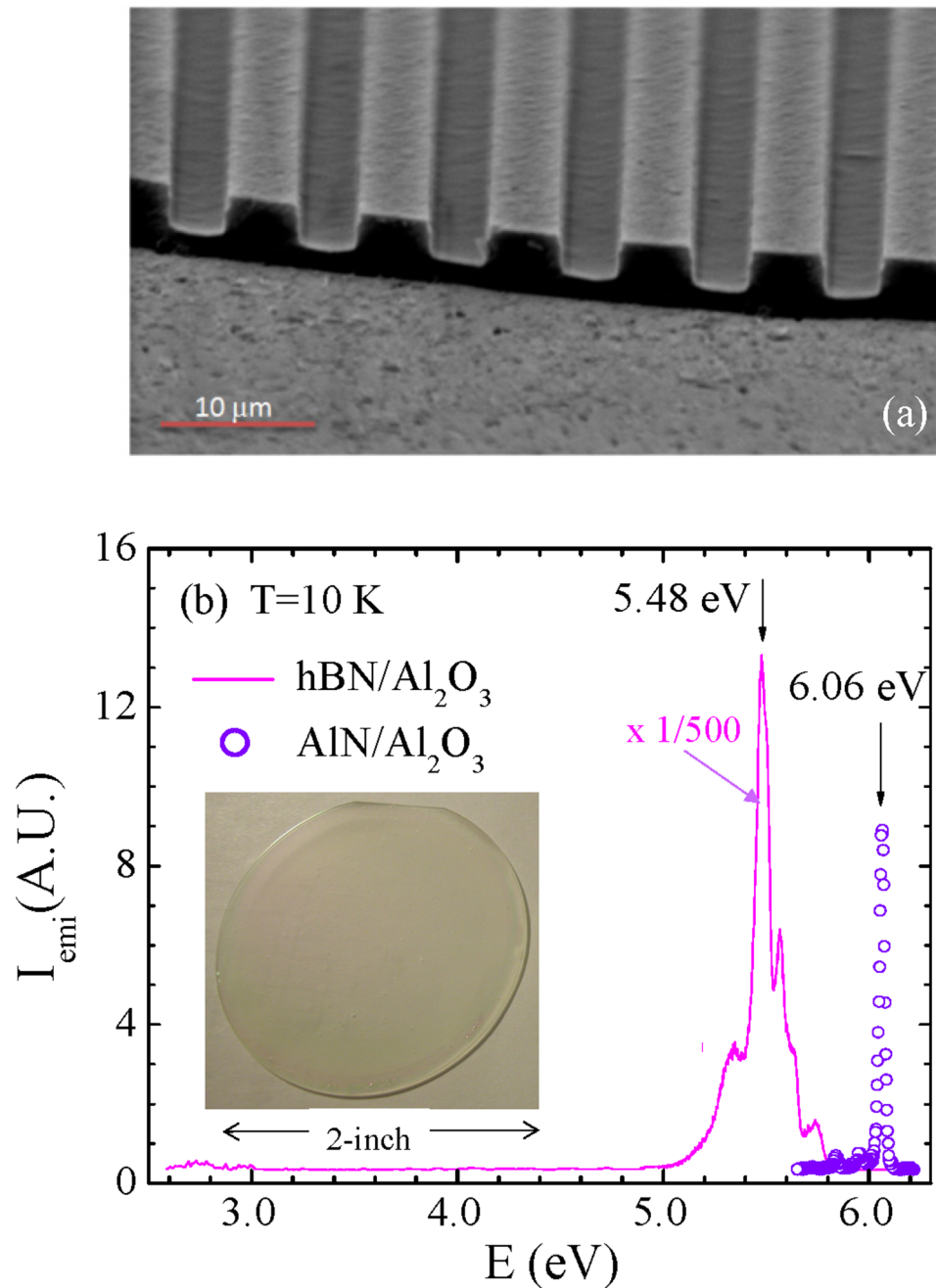


FIG. 2. (a) SEM image of an *h*BN epilayer (etched into stripes). (b) Comparison of deep UV photoluminescence spectra of *h*BN and AlN epilayers measured at 10 K. The inset is an optical image of a 2-inch wafer of *h*BN epilayer [partially reproduced from Fig. 1 of Ref. 16].

55.06°, and 88.00°, respectively with no other visible peaks. The results revealed a *c*-lattice constant $\sim 6.67 \text{ \AA}$ that matches closely with the bulk *c*-lattice constant of *h*BN ($c=6.66 \text{ \AA}$) and demonstrated that our MOCVD grown *h*BN films are single crystals in hexagonal phase.³ Figure 1(d) compares the XRD rocking curves (ω -scans) of the (0002) diffraction peaks of an *h*BN epilayer and AlN epilayer which has a comparable bandgap as *h*BN.¹⁶ Although the observed full width at half maximum (FWHM) of 380 arcsec for *h*BN epilayer is much broader than the typical FWHM (~ 63 arcsec) of high quality AlN epilayers grown by our group, but is comparable to the typical value for GaN epilayers grown on sapphire with a similar thickness.¹⁴ The comparison XRD results between

*h*BN and AlN are an indicative of the fact that the development of *h*BN epitaxial layers is in its early stage and improvements are still needed. Secondary ion mass spectrometry results also revealed that *h*BN epilayers have excellent stoichiometry.³ The grown epilayers also have a good surface morphology as indicated by the AFM image shown in Fig. 1(b) as well as by an SEM image shown in the inset of Fig. 2(a) for an *h*BN epilayer (etched into stripes). Moreover, as shown in Fig. 2(b), the measured 10 K band edge photoluminescence (PL) emission intensity of *h*BN is more than 2 orders of magnitude higher than that of high quality AlN, originating from the unusually strong $p \rightarrow p$ -like transitions and its “two-dimensional” nature.⁴ However, the presence of stacking faults, dislocations, and native defects cannot be precluded and all could contribute to the broadening of the FWHM of the XRD rocking curve.

III. RESULTS AND DISCUSSION

Van der Pauw–Hall method¹⁷ was employed to measure the electrical resistivity, carrier concentration, and mobility. To minimize the impact of possible sample inhomogeneity on the measured carrier type and mobility while employing the Van der Pauw–Hall method, we used four small size triangular ohmic contacts fabricated on the four corners of the sample.^{16,18} Ohmic contacts consist of Ni/Au (20 nm/30 nm) bilayers were deposited using e-beam evaporation followed by rapid thermal annealing at 800 °C for 10 minutes. Figure 3(a) is the microscope image of a fabricated *h*BN sample with four ohmic contacts on the corners. The ratio of the contact size (d) to the sample length (L) is $\sim 1/10$, a configuration that is considered to be adequate to provide reliable measurement results.¹⁸ Ohmic behavior of Ni/Au bilayer contacts on *h*BN is demonstrated by the linear behavior of the I-V curve shown in Fig. 3(b). However, the estimated room temperature resistivity of undoped *h*BN epilayers is in the order 10^{11} Ω -cm based on the I-V characteristics. Due to the high resistivity of these undoped samples, it was difficult to carry out Hall effect measurements below 700 °K.

At $T > 700$ °K, the mobility data consistently revealed that undoped *h*BN epilayers are semiconductors of weak p-type, similar to the case of diamond. Figure 4 summarizes the temperature dependence of the hole concentration (p), hole mobility (μ), and the p-type resistivity (ρ), measured from 700 to 790 °K. In order to determine the acceptor energy level, an Arrhenius plot of the measured free hole concentration is shown in Fig. 5. The solid line is the least squares fit of data by

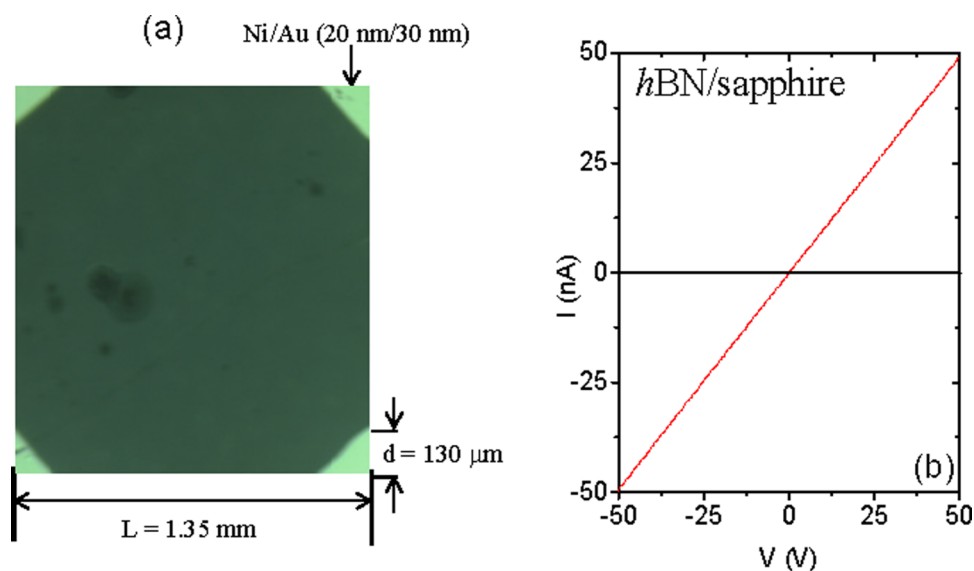


FIG. 3. (a) Optical image of an *h*BN epilayer with ohmic contacts fabricated on the four corners for Hall-effect measurements. (b) Room temperature I-V characteristics of an *h*BN epilayer obtained by employing Ni/Au bilayer (20 nm/30 nm) as ohmic contacts.

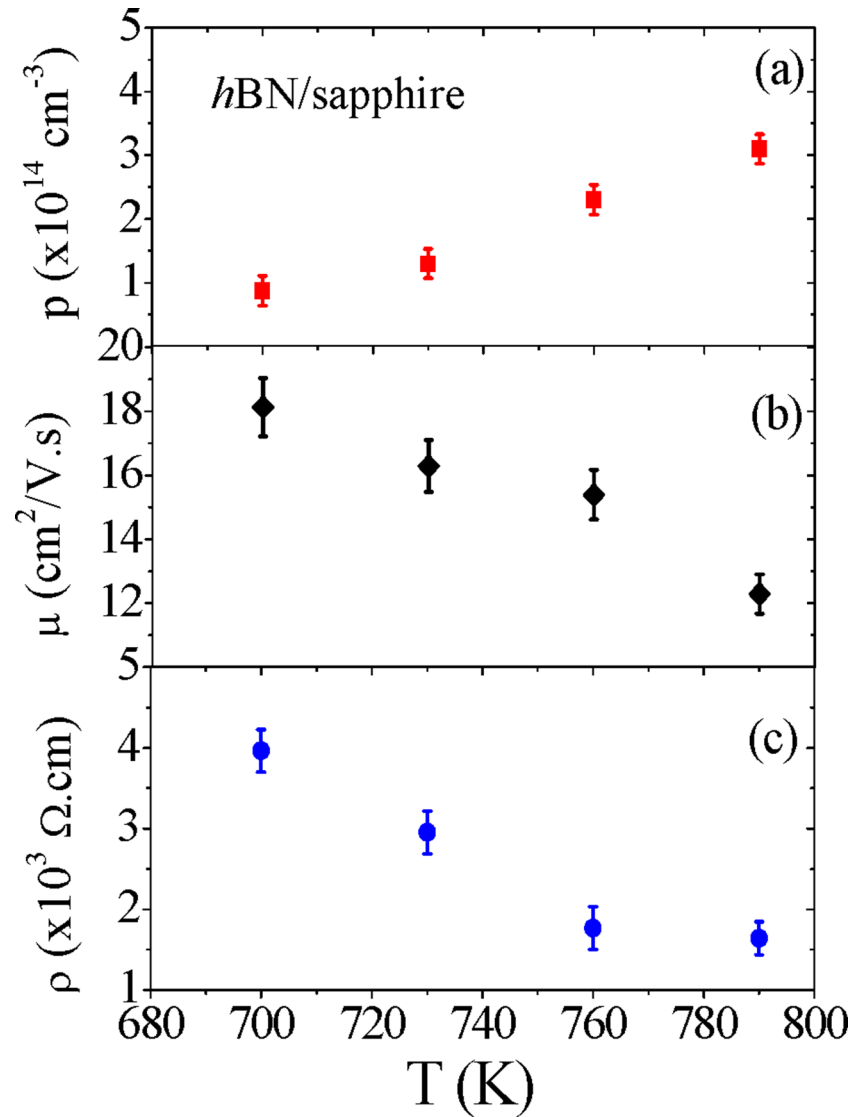


FIG. 4. The temperature dependence of the (a) hole concentration (p), (b) hole mobility μ , and (c) p-type resistivity ρ . The experimental error bars are indicated in the figures.

the following equation:

$$p = CT^{3/2}e^{-\frac{E_A}{k_B T}}, \quad (1)$$

where $k_B = 8.625 \times 10^{-5}$ ($\text{eV}\cdot\text{K}^{-1}$) is the Boltzmann's constant. The fitted value of $E_A = 0.68$ eV is the measure of the acceptor energy level above the valence band. Since the *h*BN epilayer used for this study is undoped, the origin of this deep acceptors is most likely related to the presence of native defects. One possibility is the presence of boron vacancies, V_B , or V_B related defects, which act as acceptors, in analogous to the acceptor-like native defects in III-nitrides, namely gallium vacancy, V_{Ga} , in GaN and V_{Al} in AlN.^{15,19,20}

In contrast to conventional III-nitride semiconductors, which have an isotropic wurtzite structure, *h*BN is a layer structured material. In wurtzite structure, the distances between the nearest and the second nearest neighbors are nearly the same in the directions of parallel and perpendicular to the *c*-axis. The lattice-vibration or phonon properties and hence the carrier transport properties of conventional III-nitrides therefore are isotropic (or slightly anisotropic). It is well known that the

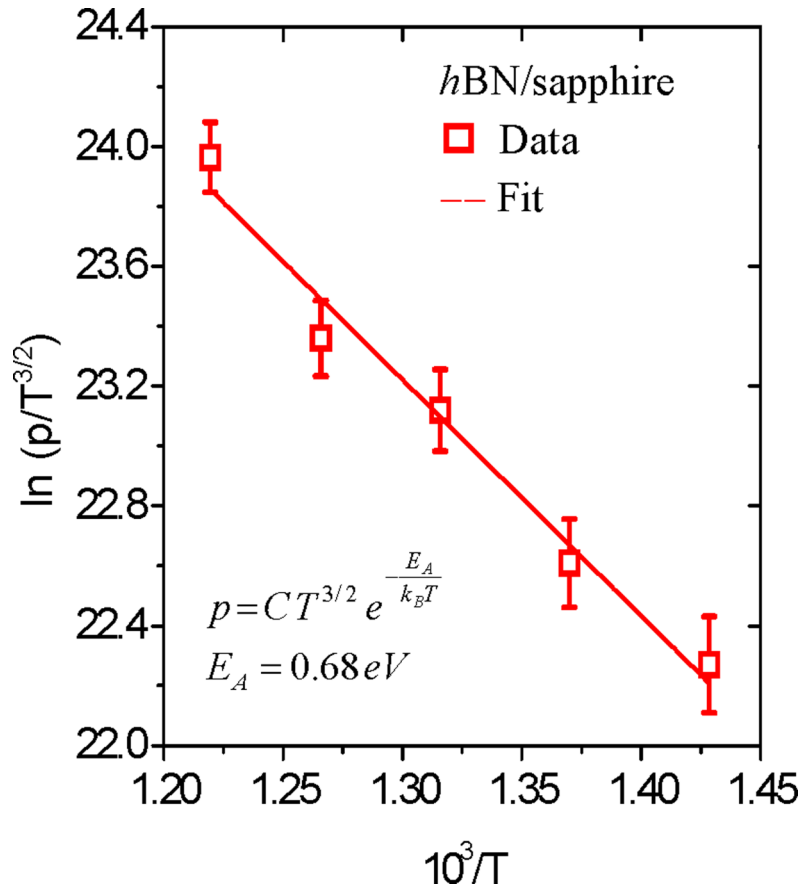


FIG. 5. The Arrhenius plot of the hole concentration. The open squares are the measured data and the solid line is the least squares fit of data with Eq. (1). The error bars for the measured data are indicated in the plot.

carrier mobility (μ) in an isotropic semiconductor typically decreases with an increase of temperature at high temperatures following a power-law dependence, $\mu \sim T^{-\alpha}$ with the exponent $\alpha \approx 1.5$ limited by acoustic phonon scattering or $\alpha \approx 0.5$ limited by optical phonon scattering.²¹

The layer structured *hBN* on the other hand has the same crystal structure as graphite with lattice constants $a = 2.54 \text{ \AA}$ and $c = 6.66 \text{ \AA}$. Consequently, like graphite its physical properties are expected to be anisotropic.^{22–26} For instance, although *hBN* bulk crystals and epilayers are three-dimensional (3D) systems, the interlayer optical transitions are much weaker than those within the layers⁴ and the exciton properties of 3D *hBN* can be described in a 2D framework.⁵ Due to the highly anisotropic nature of *hBN*, it is also expected that phonons propagate more quickly in the *c*-plane (\perp *c*-axis) with strong B-N bonds and slower along the *c*-axis (\parallel *c*-axis) with Van der Waals bonds. Furthermore, the free charge carriers also have higher mobility in the lateral direction (\perp *c*-axis) than in the vertical direction (\parallel *c*-axis). Consequently, the charge carriers can be treated approximately as if they are transporting through a stack of independent layers of a 2D structure.^{22–26} On the other hand, compared to other layered semiconductors such as GaSe, MoS₂, MoSe₂, and WSe₂,^{23–25} which typically have an energy bandgap $E_g \sim 2 \text{ eV}$ with a maximum optical phonon energy $\hbar\omega \sim 60 \text{ meV}$, *hBN* is composed of light elements B and N and has a much larger bandgap ($E_g \sim 6.4 \text{ eV}$)⁵ as well as a much larger maximum longitudinal optical (LO) phonon energy of $\hbar\omega \sim 190 \text{ meV}$.^{22,27} In fact, *hBN* may possess the largest phonon energy among all semiconductors. These unique properties together significantly influence the carrier-phonon scattering and hence the carrier transport properties, especially at high temperatures.

It has been reported that the scattering is dominated by homopolar optical phonons in layer structured semiconductors with energy gaps around 2 eV,^{23–26} in which the temperature dependence

follows $\mu \sim T^{-\alpha}$ with much large exponents than in 3D and isotropic semiconductors. For instance, $\alpha \approx 2.1$ for GaSe and $\alpha \approx 2.6$ for MoS₂ have been measured.²⁴⁻²⁶ In the weak carrier-optical phonon coupling regime, the excess carriers behave as free quasi-particles. At sufficiently high temperatures, it is well-known that the carrier-optical phonon scattering dominates in layer structured materials and the dependence of the carrier mobility on temperature can be described by²⁴⁻²⁶

$$\mu = \mu_0 T^{-\alpha} \quad (2)$$

over a certain temperature range around a characteristics temperature T_0 , where

$$\alpha = \frac{\hbar\omega}{k_B T_0} \frac{e^{\frac{\hbar\omega}{k_B T_0}}}{e^{\frac{\hbar\omega}{k_B T_0}} - 1} \approx \frac{\hbar\omega}{k_B T_0}, \quad (\hbar\omega \gg k_B T_0), \quad (3)$$

and μ_0 is the prefactor in the carrier mobility versus temperature relation and $\hbar\omega$ is the maximum phonon energy, which dictates the carrier-phonon scattering at high temperatures. Figure 6 shows the temperature dependence of the hole mobility in a natural logarithmic plot. The solid line is the least squares fit by Eq. (2). The fitted value of $\alpha = 3.02$, which is larger than those seen in GaSe ($\alpha = 2.1$) and MoS₂ ($\alpha = 2.6$). This is expected from Eq. (3) since α increases linearly with $\hbar\omega$, the maximum phonon energy. The maximum phonon energy in *h*BN is around 196 meV,^{22,27} which gives:

$$T_0 = \frac{\hbar\omega}{k_B \alpha} = \frac{\hbar\omega}{k_B T_{300} \alpha} T_{300} = \frac{196 \text{ meV}}{25 \text{ meV} \times 3.02} \times 300 = 780 \text{ }^\circ\text{K}.$$

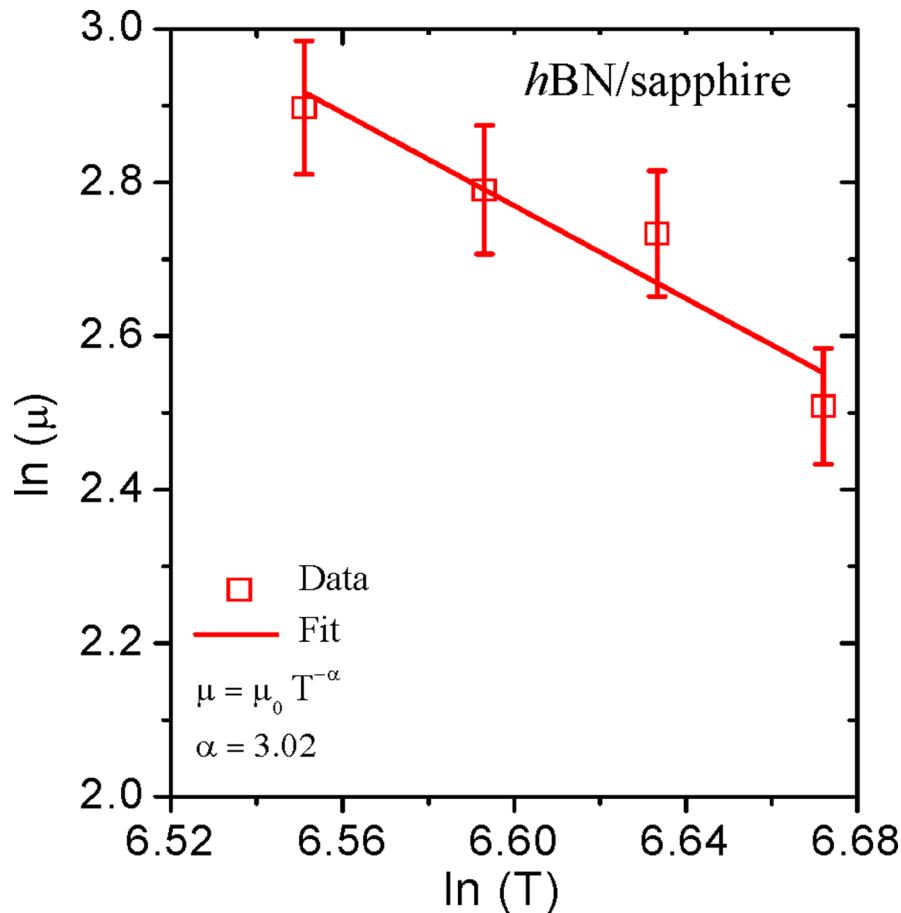


FIG. 6. $\ln(\mu)$ versus $\ln(T)$ plot of the temperature dependence of the hole mobility. The open squares are the measured data and the solid line is the least squares fit of data with Eq. (2). The error bars for the measured data are indicated in the plot.

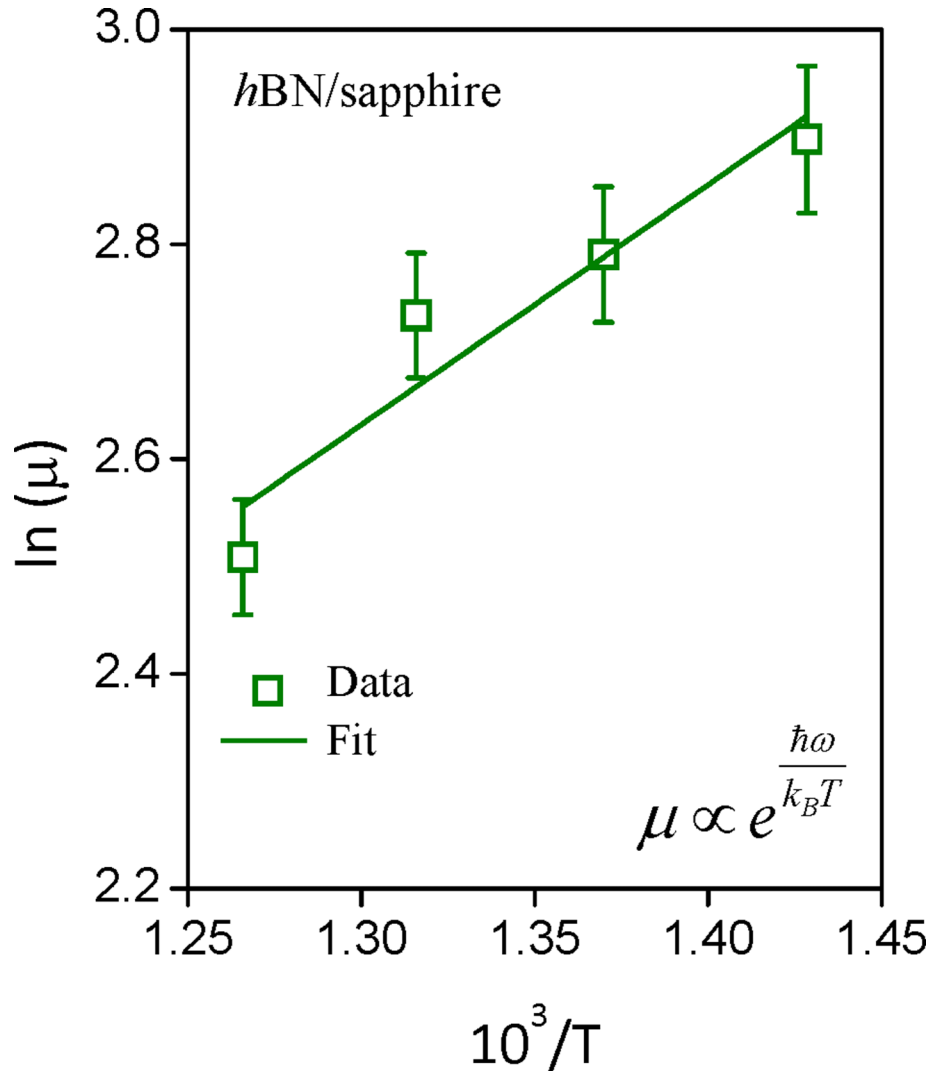


FIG. 7. A semi-logarithmic plot ($\ln(\mu)$ versus T) for the temperature dependence of the hole mobility. The open squares are the measured data and the solid line is the least squares fit of data with Eq. (4). The error bars for the measured data are indicated in the plot.

On the other hand, the maximum phonon energy in *h*BN can be estimated from the experimental data. At temperatures at which $k_B T$ is much smaller than the maximum optical phonon energy, the in-plane mobility of charge carriers in layered semiconductor due to phonon scattering satisfies the 2D limit:^{24–26}

$$\mu \propto e^{\frac{\hbar\omega}{k_B T}}, \quad (\hbar\omega \gg k_B T). \quad (4)$$

In Fig. 7, the temperature dependence of the holes mobility is presented in an Arrhenius plot according to Eq. (4). The fitting between the experimental data and Eq. (4) provides the energy of the optical phonon $\hbar\omega \approx 192$ meV (or 1546 cm^{-1}), which agrees quite well with a value of 196 meV for the maximum optical phonon energy in *h*BN measured using Raman and infrared reflection spectroscopy.^{21,27,28} The maximum eigenfrequencies of LO phonons for in-plane vibration with $k \approx 0$ is proportional to the constant forces between the nearest neighbors in-plane and inversely proportional to the reduced mass of boron and nitrogen.²¹ Due to the very large in-plane constant force and relatively small reduced mass, the maximum LO phonon energy of *h*BN is therefore larger than those in other layered semiconductors with smaller energy bandgap.^{24–26}

IV. CONCLUSIONS

In summary, single crystal *h*BN epilayers have been synthesized by MOCVD and their electrical transport properties have been studied via high temperature Hall effect measurements. It was found that undoped *h*BN epilayers exhibit weak p-type at high temperatures ($T > 700$ °K) with an in-plane resistivity of $\sim 1.6 \times 10^3 \Omega\text{-cm}$ at 790 °K. The measured energy level of the p-type defects is around 0.68 eV with a possible origin attributing to boron vacancies V_B , or V_B related defects. It was found that the temperature dependence of the hole mobility in *h*BN epilayers is dominated by the polar optical phonon scattering at high temperatures, following the power law dependence of $\mu \sim T^{-\alpha}$ with an unusually large exponent α (≈ 3.02). The observed strong optical phonon scattering is a consequence of the 2D nature or layered structure of *h*BN, which has a strong in-plane force and weak Van der Waals force between layers. The maximum energy (wave number) of the optical phonon deduced from the temperature dependent mobility is ~ 192 meV (or 1546 cm^{-1}), which agrees well with the previously reported values obtained via Raman and infrared reflectance spectroscopy. Further studies are required to gain improved understanding on the carrier transport mechanisms and conductivity control in *h*BN epilayers.

ACKNOWLEDGMENT

The effort on the electrical transport properties measurements is supported by DOE (DE-FG02-09ER46552) and the effort on structural characterization is supported by NSF (Grant No. DMR-1206652). Jiang and Lin are grateful to the AT&T Foundation for the support of Ed Whitacre and Linda Whitacre Endowed chairs.

- ¹ K. Watanabe, T. Taniguchi, and H. Kanda, *Nature Mater.* **3**, 404 (2004).
- ² K. Watanabe and T. Tanniguchi, *Phys. Rev. B* **79**, 193104 (2009).
- ³ R. Dahal, J. Li, S. Majety, B. N. Pantha, X. K. Cao, J. Y. Lin, and H. X. Jiang, *Appl. Phys. Lett.* **98**, 211110 (2011).
- ⁴ B. Huang, H. X. Jiang, X. K. Cao, J. Y. Lin, and Su-Huai Wei, *Phys. Rev. B* **86**, 155202 (2012).
- ⁵ X. K. Cao, B. Clubine, J. H. Edgar, J. Y. Lin, and H. X. Jiang, *Appl. Phys. Lett.* **103**, 191106.
- ⁶ S. Majety, X. K. Cao, J. Li, R. Dahal, J. Y. Lin, and H. X. Jiang, *Appl. Phys. Lett.* **100**, 061121 (2012).
- ⁷ M. Chubarov, H. Pedersen, H. Högberg, J. Jensen, and A. Henry, *Cryst. Growth Des.* **12**, 3215 (2012).
- ⁸ C. R. Dean, A. F. Young, I. Meric, C. Lee, L. Wang, S. Sorgenfrei, K. Watanabe, T. Taniguchi, P. Kim, K. L. Shepard, and J. Hone, *Nature Nanotechnology* **5**, 722 (2010).
- ⁹ A. K. Geim and I. V. Grigorieva, *Nature* **499**, 419 (2013).
- ¹⁰ G. F. Knoll, *Radiation Detection and Measurement*, 4th ed. (John Wiley & Sons, Hoboken, NJ, 2010).
- ¹¹ O. Osberghaus, *Zeitschrift fuer Physik* **128**, 366 (1950).
- ¹² J. Li, R. Dahal, S. Majety, J. Y. Lin, and H. X. Jiang, *Nucl. Instr. Meth. Phys. Res. A* **654**, 417 (2011).
- ¹³ T. C. Doan, S. Majety, S. Grenadier, J. Li, J. Y. Lin, and H. X. Jiang, *Nucl. Instr. Meth. Phys. Res. A* **748**, 84 (2014).
- ¹⁴ S. Nakamura, G. Fasol, and S. J. Pearton, *The Blue Laser Diode: The Complete Story* (Springer, New York, 2000).
- ¹⁵ H. X. Jiang and J. Y. Lin, *Semicon. Sci. Technol.* **29**, 084003 (2014).
- ¹⁶ S. Majety, T. C. Doan, J. Li, J. Y. Lin, and H. X. Jiang, *AIP Advances* **3**, 122116 (2013).
- ¹⁷ L. J. Van der Pauw, *Philips Research Reports* **13**, 1 (1958).
- ¹⁸ O. Bierwagen, T. Ive, C. G. Van de Walle, and J. S. Speck, *Appl. Phys. Lett.* **93**, 242108 (2008).
- ¹⁹ K. B. Nam, M. L. Nakarmi, J. Y. Lin, and H. X. Jiang, *Appl. Phys. Lett.* **86**, 222108 (2005).
- ²⁰ N. Nepal, M. L. Nakarmi, J. Y. Lin, and H. X. Jiang, *Appl. Phys. Lett.* **89**, 092107 (2006).
- ²¹ R. Geick and C. H. Perry, *Phys. Rev.* **146**, 543 (1966).
- ²² L. K. Gallos, A. N. Anagnostopoulos, and P. Argyrakis, *Phys. Rev. B* **50**, 14643 (1994).
- ²³ R. Fivaz and E. Mooser, *Phys. Rev.* **136**, A833 (1964).
- ²⁴ R. C. Fivaz, *Nuovo Cimento* **63B**, 10 (1969).
- ²⁵ *Optical and Electrical Properties*, edited by P. L. Lee (D. Reidel, Boston, 1976).
- ²⁶ J. Serrano, A. Bosak, R. Arenal, M. Krisch, K. Watanabe, T. Taniguchi, H. Kanda, A. Rubio, and L. Wirtz, *Phys. Rev. Lett.* **98**, 095503 (2007).
- ²⁷ A. C. Ferrari, J. C. Meyer, V. Scardaci, C. Casiraghi, M. Lazzeri, F. Mauri, S. Piscanec, D. Jiang, K. S. Novoselov, S. Roth, and A. K. Geim, *Phys. Rev. Lett.* **97**, 187401 (2006).
- ²⁸ A. A. Balandin, S. Ghosh, W. Bao, I. Calizo, D. Teweldebrhan, F. Miao, and C. N. Lau, *Nano Lett.* **8**, 902 (2008).